The Use of TL Detectors in Dosimetry of Systemic Radiation Therapy

A. Carita Aschan, Matti J. Toivonen, Juha S. Lampinen, Mikko Tenhunen, Kalevi J.A. Kairemo, E. Tapani Korppi-Tommola, Antti P. Jekunen, Petri Sipilä and Sauli E. Savolainen

From the Department of Physics, University of Helsinki (A.C. Aschan, J.S. Lampinen), the Departments of Radiology (A.C. Aschan, J.S. Lampinen, E.T. Korppi-Tommola, S.E. Savolainen), and Oncology (M. Tenhunen, K.J.A. Kairemo, A.P. Jekunen), Helsinki University Central Hospital, and the Finnish Centre for Radiation and Nuclear Safety (M.J. Toivonen, P. Sipilä), Helsinki, Finland

Correspondence to: Sauli Savolainen, PhD, Department of Radiology, Helsinki University Central Hospital, P.O. Box 380, FIN-00029 HYKS Helsinki, Finland. Tel: +358 9 471 2595. Fax: +358 9 471 4404. E-mail: sauli.savolainen@huch.fi

Acta Oncologica Vol. 38, No. 2, pp. 189–196, 1999

A method for determining absorbed doses to organs in systemic radiation therapy (SRT) is evaluated. The method, based on thermoluminescent (TL) dosimeters placed on the patient's skin, was validated and justified through a phantom study showing that the difference between measured (TL dosimeters in the phantom) and derived (TL method) values is within 10%. Six radioimmunotherapy (RIT) patients with widespread intraperitoneal pseudomyxoma were also studied. In dose evaluations, special emphasis was on kidneys. In addition to the TL method, the absorbed doses to kidneys were calculated using MIRD formalism and a point dose kernel technique. We conclude that in SRT the described TL method can be used to estimate the absorbed doses to those critical organs near the body surface within 50% (1 SD).

The success of systemic radiation therapy (SRT), e.g. radioimmunotherapy (RIT), is not only dependent on advances in antibody engineering, but also on the developing of accurate methods for determining dose distributions arising from internal radionuclide distributions (1, 2). To justify individual patient therapy, a treatment planning procedure is needed (3). Furthermore, it is necessary to monitor the absorbed doses that are actually delivered using independent methods. Monitoring absorbed doses is necessary for several reasons, e.g. to predetermine the risk of side effects, to use multiple dosage without cumulative risk of severe organ toxicity, and to allow escalation of the dose in individual cases. Dose estimation methods in RIT have recently been summarized by Strand et al. (1).

MIRD formalism, developed for diagnostic purposes, is a common method used to determine the dose distribution from internal radioactivity distributions (4–7). A major limitation to the procedure of using published MIRD tables (S-values) is that they do not take the variations in the size and shape of the individual anatomy into consideration, and the non-uniformity of radionuclide distribution in the source organ.

Giap et al. (8, 9) described a method for three-dimensional (3-D) internal dosimetry for RIT that integrates the 3-D activity map from SPECT (single photon emission computed tomography) with a point dose kernel technique to provide a 3-D distribution of the absorbed dose. They compared the dose calculated by their method with that measured by thermoluminescent (TL) dosimeters in a 22-cm diameter phantom and with the dose calculated using MIRD S values in an Alderson abdominal anthropomorphic phantom (8). They found that inside the phantoms the calculated absorbed doses were in good agreement with both the TL measurements and MIRD formalism. They concluded that future studies should include the validation of the 3-D method in patients receiving RIT, which requires a method of measuring absorbed dose in vivo.

Methods measuring the absorbed dose by implanting TL dosimeters into animals and tumor model systems receiving RIT have been developed (10, 11). Major limitations (12) for direct organ dose measurements with the implantation of dosimeters in critical organs (kidneys, liver, heart, lung, red marrow, etc.) are decay of detector sensitivity with time (12–14) and the need for surgical procedures. For clinical routine, the dosimeter must be placed on the skin of the patient or in accessible cavities when determining absorbed doses to critical organs.

 ISSN 0284-186X

The aim of this work was to establish an independent method for determining absorbed doses to radiosensitive organs during SRT. A method with TL dosimeters placed on the skin of the patient was therefore developed. A phantom study was carried out to establish the method. The method was used to determine the absorbed doses to a radiosensitive organ (kidney) of six patients undergoing eight RITs with ^{131}I-labeled monoclonal antibody. The measured values were compared with those obtained by using two calculation methods, one based on MIRD formalism and the other based on a point dose kernel technique (15).

MATERIAL AND METHODS

I. TLD-based patient dosimetry

TLD practice. Two TL detector types were used for the determination of absorbed doses in phantom and patient studies of this work. $CaSO_4$: Dy powder was selected for use as a gamma detector for patient studies because of its high sensitivity (TL signal per mean absorbed dose in TL material). LiF : Mg,Ti discs were used in the phantom measurements and for calibration of $CaSO_4$: Dy dosimeters because of their low energy dependence (detector sensitivity as a function of photon energy) (16).

The $CaSO_4$: Dy powder was prepared by heating at 300°C for 10 min. About 50-mg samples of the powder were then wrapped in paper for use as TL detectors. Part of the powder was reserved for calibration and background control. The LiF : Mg,Ti detectors were prepared by heating at 300°C for 10 min with rapid cooling to room temperature.

Readout of the $CaSO_4$: Dy and LiF : Mg,Ti detectors was made with the TL dosimeter reader, Toledo 654 of Vinten Instruments Ltd. (Great Britain). Equal samples of powder (20 mg) were dispensed volumetrically from each $CaSO_4$: Dy sachet for readout. The heating profiles of 135°C for 16 s followed by 25 s at 290°C or 16 s at 290°C were used for the $CaSO_4$: Dy and LiF : Mg,Ti detectors, respectively.

All LiF : Mg,Ti TL dosimeters used in this study were calibrated by irradiating dosimeters to the air kerma of 6 mGy with a ^{137}Cs source at the Secondary Standard Dosimetry Laboratory (SSDL) of Helsinki. All dosimeters were calibrated in order to avoid the need for a correction factor (eq. 1) for differences in the individual sensitivities of solid detectors. The calibration of the $CaSO_4$: Dy TL detectors was made by irradiating calibration dosimeters to the air kerma of 5 mGy with a ^{137}Cs source at SSDL of Helsinki.

Absorbed dose to a reference point. Absorbed doses to the reference points, situated on the skin surface of a patient or a phantom, D_{ref}, were calculated from the net readout values (background subtracted) of the TL detectors, r, using:

$$D_{ref} = r f_a f_{m,a} f_{D,K} C_{I,Cs} \quad [1]$$

where f_a is the air kerma calibration factor of the detectors for ^{137}Cs radiation, the factor $f_{m,a}$ (i.e. the ratio of mass energy absorption coefficients from medium to air $(\mu_{en}/\rho)_{m,a}$ (17)) converts between air kerma and medium (water or tissue) kerma, $f_{D,K}$ is a conversion factor from medium kerma to absorbed dose and $C_{I,Cs}$ is the correction factor for the difference in the detector sensitivities between the energy spectrum of ^{131}I gamma radiation at each measurement point and that of the ^{137}Cs in air.

Absorbed dose to a point inside the body. The absorbed doses to the points of interest, D_{ROI}, e.g. to those corresponding critical organs, were calculated from the absorbed doses of TL measurement points, i.e. the reference points, D_{ref}, by using:

$$D_{ROI} = f_{bolus} e^{\mu(r_{ref} - r_{ROI})} \left(\frac{r_{ref}}{r_{ROI}}\right)^2 D_{ref} \quad [2]$$

where μ is an attenuation coefficient for broad beam geometry, r_{ref} (Fig. 1) the distance from the irradiation source to the reference point, r_{ROI} (i.e. r_{kidney} in Fig. 1) the distance from the irradiation source to the region, i.e. the points of interest (ROI) and f_{bolus}, a correction factor which is defined as the ratio of the doses at the reference point in an infinite medium and the corresponding point on the surface of the patient. The factor f_{bolus} takes into account the lack of back-scattering from the bolus tissue in the reference point.

II. Phantom studies

Calibrations. An elliptical water phantom (Data Spectrum Corporation, USA) of 18.6 cm high and with long/short axis diameters of 30.5/22.0 cm was used. A cylindrical ^{131}I source (3000 MBq) diameter 5.3 cm and

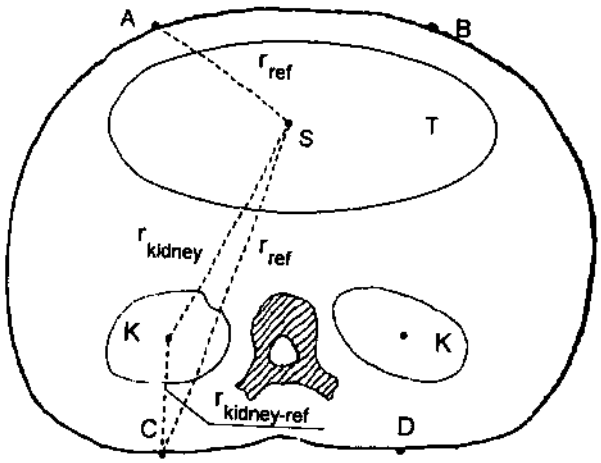

Fig. 1. A schematic illustration of the target/source volume, T: its mass centre, S; kidneys, i.e. the region of interest (ROI) and its mass centre, K: reference points A, B, C, and D; and the distances, r_{ref}, r_{kidney}, and $r_{kidney\text{-}ref}$.

Table 1

The patient data, injected activities, and the effective half-lives of the radiopharmaceutical (^{131}I-labeled monoclonal antibody B72.3) in the peritoneal cavity based on TL measurements (TLD) and gamma images (GI)

Patient	Sex	Age	Injected activity [MBq]	Half life		TLD/GI
				GI (h)	TLD (h)	
1a	Male	40	3 960	34	29	0.85
1b	Male	40	3 960	18	15	0.83
2a	Female	38	4 220	27	27	1
2b	Female	38	4 030	34	31	0.91
3	Female	57	3 870	24	23	0.96
4	Female	69	3 600	27	23	0.85
5	Female	86	3 500	27	24	0.89
6	Male	61	3 550	25	29	1.16

a = first treatment; b = second treatment.

height 8.0 cm was inserted in either a focal point or the center of the water phantom.

Dosimeter pairs of $CaSO_4$: Dy powder and LiF : Mg,Ti discs were placed on the surface of the phantom at various distances from the center of the source for derivation of the correction factors $C_{I,Cs}$ (eq. 1) for $CaSO_4$: Dy detectors at each source to detector pair distance. LiF : Mg,Ti detectors used as a pair with each $CaSO_4$: Dy detector were used for the absorbed dose measurements because of their low energy dependence. The relative sensitivities of LiF : Mg,Ti detectors to ^{131}I radiation in water as a function of distance from the source were determined by multiplying the absorbed dose fractions at each spectrum interval obtained with Monte Carlo simulation with the relative sensitivity of LiF : Mg,Ti to monoenergetic photons (16) and integrating over the entire spectrum. In Monte Carlo simulation (18) a photon beam with the energy spectrum of ^{131}I (mean energy 364 keV) was focused towards a water phantom, and the distances between the source and a target were varied.

LiF : Mg,Ti dosimeters were placed on the surface of the phantom at various distances from the center of the source for the determination of the bolus factor f_{bolus} (eq. 2). At each distance, the LiF : Mg,Ti detectors were used with and without a thick water bolus (> 10 cm) at the water–PMMA–air interface (i.e. water–air interface since PMMA, polymethylmetacrylate $(C_5H_8O_2)_n$, is nearly water equivalent for used photon energies (< 1 MeV)) for estimation of the effect of back-scattering from the bolus to the absorbed dose at the interface.

A further study was performed to confirm whether the phantom-TL material interface effects on the surface of the phantom caused by the non-equilibrium of secondary electrons have to be taken into consideration in determining absorbed doses from the readout values of the TL detectors. A monocrystalline layer of $CaSO_4$: Dy powder (few mg/cm^2) and a thick layer of the same material (> 100 mg/cm^2) were irradiated in similar geometry.

Validation of the TL method. The absorbed doses D_{ref}, measured with LiF : Mg,Ti dosimeters on the surface of the phantom, were used for validation of the TL method. The absorbed doses to the points of interest, D_{ROI}, situated at various distances from the surface of the phantom, were derived using eq. (2). Also, for comparison, the absorbed doses D_{ROI} were measured with LiF : Mg,Ti detectors situated inside the phantom at each point of interest.

III. Patient studies

Patients. Six patients (Table 1) were investigated after obtaining written informed consent, and positive radioimmunohistochemistry and immunoscintigraphy (19). The patients all had a previously diagnosed pseudomyxoma at the time of radioimmunotherapy. The patients had large intraperitoneal disease with no other current treatment available. The pseudomyxomas originated from appendixes (3 patients) or from ovaries (3 patients), and their previous treatments were 1–5 palliative laparotomies. This disease is characterized by massive mucous colloid production out of solitary cells and disseminated intraperitoneal spread with no exact tumor area that can be delineated (19). The study was approved by the Ethics Committee of the Department of Oncology, Helsinki University Central Hospital.

Radioantibody. ^{131}I-labeled monoclonal antibody B72.3 (Sorin Biomedica, Saluggia, Italy) recognizes the TAG-72 antigen on epithelial carcinomas (20, 21). IgG mouse monoclonal antibody was labeled with ^{131}I in 0.04 M phosphate buffer at pH 7.4; 10 ml of solution contained 3700 MBq ^{131}I, 7.4 mg MoAb in Na_2HPO_4, and human serum albumin. According to the manufacturer, the radiochemical purity of this solution was over 95%. The immunoreactivity of the radio-iodinated MoAb was 50–60%.

The activity was infused intraperitoneally (i.p.) in 500–1000 ml physiological saline within 1 hour.

Imaging protocol. CT images were taken from the abdominal area of each patient with a Philips SR 4000 CT scanner. The slice thickness was 1 cm and the slice separation varied from 1 to 5 cm.

The patients were imaged daily for a total of one week with a gamma camera (Siemens Phogamma) using a high-energy pinhole collimator with an AP projection at a great distance (approx. 1.5 m). The effective half-life of the activity in the abdominal cavity was derived for each patient from daily data of gamma camera images, and was estimated to be between 1 and 2 days (Table 1). The biological half-lives varied, respectively, between 20 and 41 h.

Single photon emission computed tomography and whole-body scanning were performed at 3, 10, and 24 days after i.p. injection in order to study the 3-D activity distribution in the abdominal area of the body. The imaging device was a Picker Prism 2000 dual detector gamma camera equipped with a medium energy collimator up to 300 keV. The SPECT study was performed by collecting sixty frames of 45-s acquisition time using a 64×64 matrix. The whole-body scanning speed was 10 cm/min and the matrix size was $1\ 024 \times 256$.

Measurement practice. Four reference points were marked on the skin of the patients for dose estimations. The first two (posterior) points represented the right and left kidneys, and two points were selected on the upper abdomen (Fig. 1). Measurements with $CaSO_4 : Dy$ TL dosimeters were made by taping the dosimeters on each reference point for a period of one hour. These measurements were repeated with new detectors three times during the first day, and once daily for the next five days.

The average dose rates at the moment of successive measurements, $\dot{D}_{ref}$, were derived using eq. (1), and exponential elimination curves were then fitted to the sets of dose rates corresponding to each reference point using the least squares method (Fig. 2). In order to obtain the absorbed doses for reference points, D_{ref}, the fitted (exponential) functions were integrated to infinity.

In determining D_{ROI}, CT images of the patients were used in estimating the distances, r_{ref} and $r_{ROI} = r_{kidney}$ of eq. (2) (Fig. 1). The mass center of abdominal cavity estimated from CT images was used to approximate the volume of the cancer tissue as a point source. For the patient studies, where ROI (i.e. kidney) was located close to the reference point (between the reference point and the source), r_{ref} was approximated to be $r_{kidney} + r_{kidney\text{-}ref}$, in which the latter value is the distance from the kidney to the corresponding reference point (Fig. 1). The ratio $(r_{ref}/r_{kidney})^2$ was approximated from CT images to vary from 1.3 to 2.3.

IV. Computing the cumulative absorbed dose

For the patient studies, two independent methods were used to compute the cumulative absorbed doses to the kidneys: one based on MIRD formalism and the other based on a point dose kernel technique.

The absorbed doses based on the MIRD formalism were calculated by approximating the injected activity at peritoneal cavity for which Watson et al. (22) have introduced photon S-values for several radionuclides, including ^{131}I. Residence times ($T_{\frac{1}{2}}/\ln 2$) were obtained from daily gamma image data.

The dose to kidneys caused by renal elimination of the activity was calculated using the MIRDOSE3 program (23), based on the MIRD formalism. The residence time of radionuclide in the kidneys was estimated to be the same as that for the whole body from the daily gamma image data; residence time varied between 30 and 58 h. Kidney uptake was estimated to be 0.8%/injected activity (19).

Another program (*Intdose*), which uses cumulative activity distribution, point dose kernels and convolution, was used to calculate the absorbed dose distribution. The methods used in the program have recently been described by Lampinen et al. (15). In our work, the cumulative activity distribution was taken from the third-day SPECT

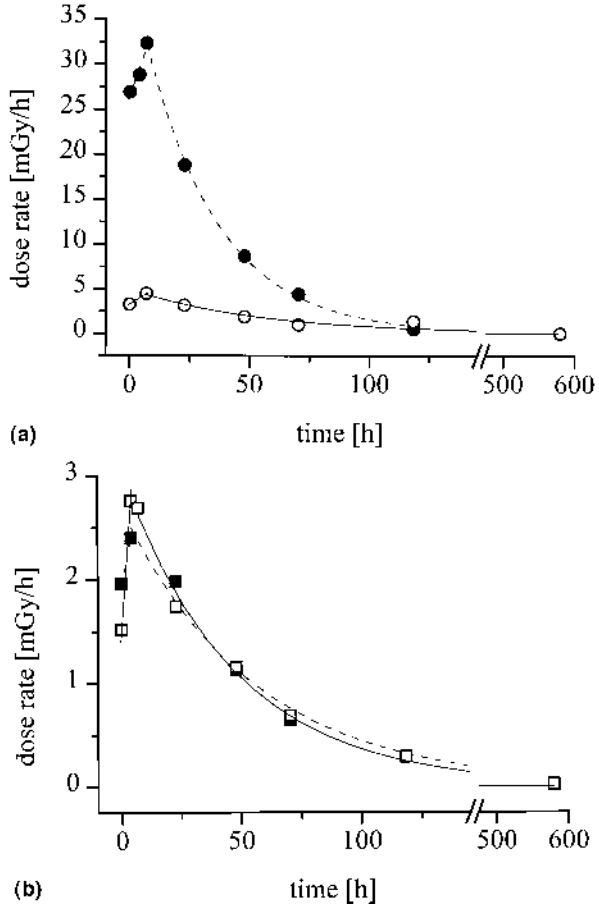

Fig. 2. The variation in dose rate after injection (a) at reference points A (●) and B (○) and (b) at reference points C (■) and D (□) (Fig. 1), corresponding to the kidneys and abdomen for patient 1.

Table 2

The absorbed doses measured, derived (TL method) and calculated (Intdose) to the points of interest (ROI) inside the phantom. The ROIs were situated at various distances from the reference points

r_{ref}	$r_{ref} - r_{ROI}$	Measured	TL method	Diff.	Measured	Intdose	Diff.
(cm)	(cm)	(mGy)	(mGy)	(%)	(mGy)	(mGy)	(%)
16	6	1 639	1 742	6	1 639	1 680	3
21.5	5.5	552	556	1	552	570	3
21.5	11.5	1 639	1 806	10			

images ($64 \times 64 \times 64$) and it was embedded in a ($128 \times 128 \times 128$) zero-matrix. The point dose kernel for ^{131}I was taken from Furhang et al. (24).

In the phantom study the calculated dose distribution was probed for absorbed doses at points of interest situated at various distances from the reference points.

In the patient studies, a typical set of CT data consisted of 13 (1 cm thick) slices of 256×256 matrices, where the pixel size was 2.0×2.0 mm^2. These slices were segmented and transformed into a volume corresponding to the SPECT data which had 64 (9.34 mm thick) slices of 64×64 matrices, with a pixel size of 5.76×5.76 mm^2. This step involved matching the CT and SPECT images on the same coordinate system. The process was carried out manually. The matrices of the absorbed dose distribution and the segmented organs were then compared and the mean dose for each organ was calculated.

RESULTS

Phantom studies

The absorbed doses measured with LiF : Mg,Ti dosimeters, placed on the surface of the phantom at the water–air interface and with those covered with a water bolus, differed by the factor f_{bolus}, which was found to be 1.25 ± 0.05. The doses as a function of distance from the source obtained from measurements with bolus-covered LiF : Mg,Ti detectors were used to determine the attenuation coefficient for broad beam geometry (including scattering), μ, the value of which was found to be 0.05 ± 0.01 cm^{-1}.

According to the Monte Carlo simulation, the average energy of ^{131}I radiation in water decreases as a function of distance from source to detector. However, the sensitivity of LiF : Mg,Ti is independent (within 1%) the source to detector distance.

The phantom study on the phantom-TL material interface showed no thickness effect in the response of $CaSO_4$:Dy powder on the surface of the phantom. Therefore, the value of 1.00 used for the factor $f_{D,K}$ in eq. (1) for measurements inside the phantom (the secondary electron equilibrium) proved to apply also to the measurements on the surface of the phantom where the requirement for the secondary electron equilibrium is not completely met.

Table 2 shows the absorbed doses measured, derived (TL method) and calculated (*Intdose*) to the points of interest (ROI) situated at various distances from the surface of the phantom. The derived absorbed doses to the ROI were obtained from TL measurements with LiF : Mg,Ti discs at the water–air interface and using eq. (2).

Patient studies

Table 1 shows that the effective half-lives of the activity in the abdominal cavity correlate ($r = 0.85$) between the derivations based on the daily gamma-image data and TL dosimeters placed on reference points A and B above the abdomen (Fig. 1). Fig. 2 shows an exponential decay of the dose-rate data.

A comparison between the absorbed doses to the kidneys derived using the TL method and calculated using MIRD formalism and a computer program based on the point dose kernel technique (*Intdose*) is presented in Table 3. These doses to the kidneys arising from the penetrating gamma component of ^{131}I are due to the activity in the tumor volume. In addition, renal elimination of the activity causes dose to the kidneys. The average dose attributable to activity passing the kidneys was found to be 152 ± 30 (1 SD) μGy/MBq, and therefore for all patients less than 0.8 Gy (Table 1).

Uncertainties of measurements with TL dosimeters

Table 4 illustrates the uncertainties of the absorbed (kidney) dose determinations present in the measurements with $CaSO_4$: Dy TL dosimeters placed on the skin of the patient. The uncertainties of the phantom study with LiF : Mg,Ti detectors are also presented.

DISCUSSION

In this work, a method to determine the absorbed doses to critical organs using TL dosimeters placed on the skin of the patients was developed. A phantom study was carried out to establish the TL method. To estimate the capabilities of the experimental TL method in the patient studies, it was necessary to examine its accuracy, and its versatility and practicality in general. In these discussions special emphasis was placed on a critical organ of the treatment, the kidney.

In the patient studies, the total uncertainty of TLD practice, and therefore the uncertainty of the absorbed dose measurements in the reference points, is found to be 8%, (1 SD). The uncertainty is mainly due to the calibration of dosimeters based on the phantom studies with $CaSO_4$: Dy and LiF : Mg,Ti detector pairs. The phantom study taking into consideration the geometry of the scattering and the measurement conditions was found necessary since the relative sensitivity of the $CaSO_4$: Dy dosimeters varies as a function of distance from the source. This is due to the energy dependence of $CaSO_4$: Dy; radiation arriving at the water–air interface has a large amount of low-energy scattered photons as a result of Compton interactions of the 364 keV gamma radiation. According to the results of the Monte Carlo simulation, the sensitivity of the LiF : Mg,Ti for ^{131}I gamma rays (364 keV) equals within 1% that for the calibration radiation (^{137}Cs) at each source to detector distance, and thus it is justifiable to use LiF : Mg,Ti detectors for determining the sensitivity of the $CaSO_4$: Dy. Furthermore, the total uncertainty of TLD practice in the phantom study in which the LiF : Mg,Ti detectors were used was only 3% (1 SD) (Table 4).

The absorbed dose to the reference point, i.e. in the tissue–air interface, lacks the contribution of the back-scattering present in the region of interest inside the body. However, for the patients' comfort no bolus was used to cover the TL dosimeters in patient measurements. Therefore, it was necessary to determine a bolus factor from the phantom study to correct the lack of back-scattering from the bolus tissue in the reference point compared to that in the region of interest. Moreover, the attenuation coefficient for broad beam geometry (including scattering) was determined from the phantom study. As is well known in SPECT applications (25, 26), the coefficient is lower from the table value of the linear attenuation coefficient for narrow beam geometry for 364 keV photons (17).

In the patient studies, uncertainty in measuring the individual distances from the (point) irradiation source to the reference point (r_{ref}) or to the point of interest (r_{ROI}) was estimated to be 20% (1 SD) (Table 4). Therefore, the uncertainties in determining $\exp[\mu r_{kidney\text{-}ref}]$ and $(r_{ref}/r_{ROI})^2$ of eq. (2) were estimated to be 20% and 28% (1 SD), respectively. The uncertainty caused by the use of a point source instead of a volume distribution of the activity incorporated in the cancer tissue was calculated (*Intdose*) to be 10% (1 SD). The *Intdose* program was also used to calculate the maximum error caused by the use of a point of interest instead of region of interest, i.e. the whole organ, in determining the absorbed dose. The error was found to be 11%. The total uncertainty of measuring absorbed doses of the organs with the TL dosimeters placed on the skin of the patient is in this study below 50% (1 SD) (Table 4). The total uncertainty is high compared with that of the phantom study (15%, 1 SD), and is mainly explained by the uncertainty in the absorbed dose in the reference point arising from the uncertain radioactivity distribution in the body (25%, 1 SD), and by the characteristics of the disease. No exact tumor area can be delineated, and therefore the measuring distances from the (point) irradiation source to the reference point (r_{ref}) or to the point of interest (r_{ROI}) are uncertain.

It appears from Table 2 that the percentage point differences between the measured and derived (TL method) absorbed doses to the points of interest situated at the short distance of approx. 6 cm from the surface of the phantom are below 10%. However, when the distance from the reference point to point of interest ($r_{ref} - r_{ROI}$) is longer (> 10 cm), the difference between measured and derived values increases. Therefore, according to the phantom study, the method of measuring the absorbed doses to the organs with TL dosimeters placed on the skin of a patient is justified with short ($r_{ref} - r_{ROI}$) -distances.

Table 3

The absorbed doses per injected activity to kidneys derived using the TL method and calculated using MIRD formalism and a computer program based on the point dose kernel technique (Intdose)

Patient	Right kidney			Left kidney			Kidneys*		
	TLD (μGy/MBq)	Intdose	Diff. (%)	TLD (μGy/MBq)	Intdose	Diff. (%)	TLD (μGy/MBq)	MIRD	Diff. (%)
1a	111	139	−25	104	146	−41	109	212	−95
1b	40	141	−250	38	146	−287	40	111	−175
2a	69	235	−241	76	194	−156	73	168	−129
2b	112	196	−76	99	216	−118	107	211	−98
3	83	nd	nd	109	nd	nd	96	150	−57
4	86	89	−3	83	89	−7	86	169	−97
5	349	189	46	151	186	−23	251	169	33
6	59	118	−100	73	121	−65	68	155	−129

a: First treatment; b: second treatment; nd; for technical reasons no data available.
* Average of two kidneys.

Table 4

A summary of the components of the uncertainties and the combined uncertainties of the absorbed doses measured with TL detectors to the points of interest

Specification of the uncertainty u_i	Reference equation	Phantom Estimated u_i (1 SD) %	Patient
$u_1 = u(rf_a f_{m,a} f_{D,K})$	1	3	3
$u_2 = u(C_{I,Cs})$	1	1	7
$u_3 = u(D_m) = (u_1^2 + u_2^2)^{1/2}$	1	3	8
$u_4 = u(D_{ref}) = u_3$	2	3	8
$u_5 = u(f_{bolus})$	2	4	4
$u_6 = u(r_{ref}) = u(r_{ROI})$	2	5	20
$u_7 = u(r_{ref} - r_{ROI})$	2	10	40
$u_8 = u(\exp[\mu(r_{ref} - r_{ROI})])$	2	8	20
$u_9 = u((r_{ref}/r_{ROI})^2)$	2	7	28
$u_{10} = u$(point score)		10	10
$u_{11} = u$(dose in a point)		0	11
$u_{12} = u$(activity distribution)		0	25
$u_{13} = u(D_{ROI}) = (u_4^2 + u_5^2 + u_8^2 + u_9^2 + u_{10}^2 + u_{11}^2 + u_{12}^2)^{1/2}$	2	15	46

It appears from Table 3 that there is a systematic trend toward the computed (*Intdose* and MIRD formalism) absorbed doses to the kidneys of the patients being higher than those measured with TL dosimeters. In addition to the above-mentioned uncertainties of TL measurements, the difference may be due to the dynamic conditions of the patient studies; when computing the absorbed doses, a static activity distribution until total decay was assumed.

The uncertainties in calculations based on MIRD formalism are due to the assumption of a uniform radionuclide distribution in the peritoneal cavity and the differences between individual anatomies and a modified version of the Fisher-Snyder phantom (27) used by Watson et al. (22). By comparing the thickness of the patients in this study (swollen by the disease) to that of the Fisher-Snyder phantom (20 cm, short axis), the over-estimation of absorbed kidney doses arising from the anatomical differences was estimated to be on average 25%. The total uncertainty of the calculations based on MIRD formalism was estimated to be approx. 50–60% in this study.

The sources of error in the *Intdose* results are mainly associated with the method used to quantify the activity and with matching the CT and SPECT images on the same coordinate system. Quantification of ^{131}I is difficult. Even if scatter and attenuation corrections had been done, the biodistribution of the isotope would still be unknown. *Intdose* calculations neglect (i) all the activity circulating in the blood (outside the SPECT slices), (ii) activity in the thyroid, and (iii) any changes in the biodistribution during the treatment. In static conditions of the phantom, *Intdose* calculations agree well with TL measurements (Table 2). Therefore, large discrepancies in patient doses calculated with *Intdose* and derived through the TL method indicate the great influence of the changes in biodistribution. In terms of dose calculations, ^{131}I is badly suited for SRT. As for matching the CT and SPECT images, the use of a registration technique (28) is recommended in order to minimize the workload and uncertainties associated with image manipulation.

The effective half-lives of the radiopharmaceutical in the abdominal cavity were essentially smaller than the physical half-life of ^{131}I (8.04 d) for all patients (Table 1). Planar AP images revealed a clear activity in the thyroid, which indicated that there was free iodine in the body due to in vivo dehalogenation. The activity observed from planar AP images in the urinary bladder indicated that the activity passed through the kidneys, causing an internal absorbed kidney dose estimated to be less than 0.8 Gy. The total absorbed dose to the kidneys was less than 1.5 Gy for all patients. In this study, the kidney was considered as an example of a radiosensitive organ but, in addition, red marrow is the dose-limiting organ in most implementations of RIT (29, 30).

An important advantage of measuring absorbed doses as a result of penetrating gamma radiation by TL dosimeters on the skin of the patient is its simplicity; the method is convenient for the patient because it does not require surgery. According to our results, despite its simplicity, the method is accurate enough to estimate the absorbed doses to those organs near the body surface (kidneys, liver, heart, etc.). $CaSO_4$: Dy is sufficiently sensitive TL material, but a complicated calibration procedure is needed because of its energy-dependent response. Highly sensitive LiF : Mg,Cu,P (31, 32) dosimeters might be more appropriate for the method described in this paper, but their use in clinical applications is limited because of the critical annealing procedure needed in preparing the dosimeters for reuse.

It is concluded that, as an independent measurement technique, the described method based on TL dosimeters is suited to the control of treatment and treatment planning procedures. The method is also versatile: it gives half-lives as well as absorbed doses, with crude prognoses of these quantities already available the second day after the treatment infusion.

ACKNOWLEDGEMENTS

The authors express their appreciation to Eero Salli, M.Sc.(Eng.), for his technical assistance. The work was supported by the Academy of Finland, University of Helsinki, the State Subsidy for University Hospitals, research grant of the Departments of Radiology and Neurology, Helsinki University Central Hospital (ACA, JSL, SES) and the Finnish Society of Nuclear Medicine (ACA, JSL).

REFERENCES

1. Strand S-E, Jönsson B-A, Ljungberg M, Tennvall J. Radioimmunotherapy dosimetry—a review. Acta Oncol 1993; 32: 807–17.
2. Chatal JF, Peltier P, Bardies M, et al. Does immunoscintigraphy serve clinical needs effectively? Is there a future for radioimmunotherapy? Eur J Nucl Med 1992; 19: 205–13.
3. Erdi AK, Erdi YE, Yorke ED, Wessels BW. Treatment planning for radio-immunotherapy. Phys Med Biol 1996; 41: 2009–26.
4. International Commission on Radiation Units and Measurements. Methods of assessment of absorbed dose in clinical use of radionuclides. Washington, DC: ICRU Report No. 32, 1979.
5. Loevinger R, Berman M. A revised schema for calculating the absorbed dose from biologically distributed radionuclides. MIRD Pamphlet No. 1, Revised, New York: The Society of Nuclear Medicine, 1976.
6. Snyder WS, Ford MR, Warner GG, Watson SB. 'S', Absorbed dose per unit cumulative activity for selected radionuclides and organs. MIRD Pamphlet No. 11, New York: The Society of Nuclear Medicine, 1975.
7. Watson EE, Stabin MG, Siegel JA. MIRD formulation. Med Phys 1993; 20: 511–4.
8. Giap HB, Macey DJ, Bayouth JE, Boyer AL. Validation of a dose-point kernel convolution technique for internal dosimetry. Phys Med Biol 1995; 40: 365–81.
9. Giap HB, Macey DJ, Podoloff DA. Development of a SPECT-based three-dimensional treatment planning system for radioimmunotherapy. J Nucl Med 1995; 36: 1885–94.
10. Griffith MH, Yorke ED, Wessels BW, DeNardo GL, Neacy WP. Direct dose confirmation of quantitative autoradiography with micro-TLD measurements for radioimmunotherapy. J Nucl Med 1988; 29: 1795–809.
11. Wessels BW, Griffith MH. Miniature thermoluminescent dosimeter absorbed dose measurements in tumor phantom models. J Nucl Med 1986; 27: 1308–14.
12. Strandh M, Strand S-E. In vivo absorbed dose measurements with mini-TLDs. Parameters effecting the reliability. Acta Oncol 1996; 35: 713–9.
13. Strand S-E, Strandh M, Spanne P. Electron microscopy and computed microtomography studies of in vivo implanted mini-TL dosimeters. Acta Oncol 1993; 32: 787–91.
14. Demidecki AJ, Williams LE, Wons JYC, et al. Considerations on the calibration of small thermoluminescent dosimeters used for measurement of beta particle absorbed doses in liquid environments. Med Phys 1993; 20: 1079–87.
15. Lampinen JS, Pohjonen HK, Savolainen SE. Calculating internal dose by convolution from SPECT/MR fusion images. Ann Nucl Med 1998; 12: 1–7.
16. Bassi P, Busuoli G, Rimondi O. Calculated energy dependence of some RTL and RPL detectors. Int J of Appl Radiat Isot 1976; 27: 291–305.
17. Hubbell JH. Photon mass attenuation and energy-absorption coefficients from 1 keV to 20 MeV. Int J Appl Radiat Isot 1982; 33: 1269–90.
18. Nelson WR, Hirayama H, Rogers DWO. The EGS4 code system. Stanford Linear Accelerator Center Report SLAC-265; 1985.
19. Kairemo KJA, Jekunen AP, Bondestam S, Korppi-Tommola ET, Savolainen S, Paavonen TK. Detection of pseudomyxoma peritonei with radioimmunohistochemistry and radioimmunoscintigraphy. Cancer Biother Radiopharm 1996; 11: 325–34.
20. Colcher D, Horan-Hand P, Nuti M, Schlom J. A spectrum of monoclonal antibodies reactive with human mammary tumor cells. Proc Natl Acad Sci USA 1981; 78: 3199–203.
21. Johnson VG, Schlom J, Paterson AJ, Bennett J, Magnani JL, Colcher D. Analysis of a human tumor-associated (TAG-72) identified by monoclonal antibody B72.3. Cancer Res 1986; 46: 850–7.
22. Watson EE, Stabin MG, Davis JL, Eckerman KF. A model of the peritoneal cavity for use in internal dosimetry. J Nucl Med 1989; 30: 2002–11.
23. Stabin MG. MIRDOSE: Personal computer software for internal dose assessment in nuclear medicine. J Nucl Med 1996; 37: 538–46.
24. Furhang EE, Sgouros G, Chui C-S. Radionuclide photon dose kernels for internal emitter dosimetry. Med Phys 1996; 23: 759–64.
25. Larsson SA. Gamma camera emission tomography. Acta Radiol 1980; (Suppl 363): 75.
26. Harris CC, Greer KL, Jaszczak RJ, Floyd CE Jr, Fearnow EC, Coleman RE. Tc-99m attenuation coefficient in water-filled phantoms determined with gamma cameras. Med Phys 1984; 11: 681–5.
27. Christy M, Eckerman K. Specific absorbed fractions of energy at various ages from internal photon sources. ORNL/TM-8381. Oak Ridge, TN: Oak Ridge National Laboratory, 1987.
28. Pohjonen HK, Savolainen SE, Nikkinen PH, Poutanen V-PO, Korppi-Tommola ET, Liewendahl BK. Abdominal SPECT/MRI fusion applied to the study of splenic and hepatic uptake of radiolabeled thrombocytes and colloids. Ann Nucl Med 1996; 10: 409–17.
29. Sgouros G. Bone marrow dosimetry for radioimmunotherapy: theoretical considerations. J Nucl Med 1993; 34: 689–94.
30. Vriesendorp HM, Quadri SM, Andersson BS, Dicke KA. Hematologic side effects of radiolabeled immunoglobulin therapy. Exp Hematol 1996; 24: 1183–90.
31. Bilski P, Olko P, Burgkhardt B, Piesch E, Waligorski MPR. Thermoluminescence efficiency of LiF:Mg,Cu,P (MCP-N) detectors to photons, beta electrons, alpha particles and thermal neutrons. Radiat Prot Dosim 1994; 55: 31–8.
32. Horowitz YS, Shachar BB. Thermoluminescent LiF (Mg, Cu, P) for gamma ray dosimetry in mixed fast neutron-gamma ray radiation fields. Radiat Prot Dosim 1988; 23: 401–4.